



RESEARCH ARTICLE

# Sensorless model-based tension control for a cable-driven exosuit

Elena Bardi<sup>1,2</sup> , Adrian Esser<sup>3</sup> , Peter Wolf<sup>3</sup>, Marta Gandolla<sup>1,2</sup>, Emilia Ambrosini<sup>1,4</sup>,  
Alessandra Pedrocchi<sup>1,4</sup> and Robert Riener<sup>3</sup>

<sup>1</sup>WeCobot Lab, Polo territoriale di Lecco, Politecnico di Milano, Milano, Italy

<sup>2</sup>Department of Mechanical Engineering, Milano, Italy

<sup>3</sup>Sensory Motor Systems Lab, Department of Health Sciences and Technology, ETH Zürich, Zürich, Switzerland

<sup>4</sup>NEARLab, Department of Electronics, Informatics and Bioengineering, Politecnico di Milano, Milano, Italy

**Corresponding author:** Adrian Esser; Email: [adrian.esser@hest.ethz.ch](mailto:adrian.esser@hest.ethz.ch)

**Received:** 27 June 2024; **Revised:** 13 September 2024; **Accepted:** 06 October 2024

**Keywords:** Soft wearable robotics; Exosuits; Human-robot interaction; Rehabilitationrobotics; Control

## Abstract

Cable-driven exosuits have the potential to support individuals with motor disabilities across the continuum of care. When supporting a limb with a cable, force sensors are often used to measure tension. However, force sensors add cost, complexity, and distal components. This paper presents a design and control approach to remove the force sensor from an upper limb cable-driven exosuit. A mechanical design for the exosuit was developed to maximize passive transparency. Then, a data-driven friction identification was conducted on a mannequin test bench to design a model-based tension controller. Seventeen healthy participants raised and lowered their right arms to evaluate tension tracking, movement quality, and muscular effort. Questionnaires on discomfort, physical exertion, and fatigue were collected. The proposed strategy allowed tracking the desired assistive torque with a root mean square error of 0.71 Nm (18%) at 50% gravity support. During the raising phase, the electromyography signals of the anterior deltoid, trapezius, and pectoralis major were reduced on average compared to the no-suit condition by 30, 38, and 38%, respectively. The posterior deltoid activity was increased by 32% during lowering. Position tracking was not significantly altered, whereas movement smoothness significantly decreased. This work demonstrates the feasibility and effectiveness of removing the force sensor from a cable-driven exosuit. A significant increase in discomfort in the lower neck and right shoulder indicated that the ergonomics of the suit could be improved. Overall this work paves the way toward simpler and more affordable exosuits.

## 1. Introduction

### 1.1. Motivation of the study

Impairments of the upper limb(s) may result from conditions, such as stroke, spinal cord injury, muscular dystrophy, multiple sclerosis, amyotrophic lateral sclerosis, and ageing, and might strongly affect the ability to conduct daily activities autonomously (Bohannon, 2007; Nätterlund and Ahlström, 2001; Wang et al., 2020). Motor rehabilitation is fundamental in addressing the loss of any ability (Faria-Fortini et al., 2011). In cases where complete recovery is unattainable, individuals may require support with everyday

activities through the use of assistive devices, which aim to restore independence to individuals with disabilities (Longatelli et al., 2021; Readioff et al., 2022).

In the field of assistive wearable robotics, there is a growing interest in soft wearable devices, referred to as exosuits (Georgarakis et al., 2022; Noronha et al., 2022; Proietti et al., 2023). Key features of exosuits include being lightweight, portable, comfortable, and less constraining for natural movements, making them suitable for daily use (Bardi et al., 2022; Xiloyannis et al., 2021). Among the possible exosuit types, such as pneumatic (Das and Kurita, 2020; Proietti et al., 2023), direct current (DC) motor-based cable-driven (or tendon-driven) exosuits are promising because of the maturity of the technology and the possibility of locating the control and actuation units proximally on the body.

A non-located load cell is often used to measure the cable tension in exosuits (Choi et al., 2019; Georgarakis et al., 2022; Hosseini et al., 2020; Wu et al., 2018; Xiloyannis et al., 2019). A common control framework, referred to as indirect force control (Calanca et al., 2016), closes an outer force loop on the load cell and an inner velocity loop on the motor encoder to render a desired interaction force. Directly measuring the output tension of a tendon driver unit (TDU) allows for disturbances, such as motor inertia and transmission friction, to be compensated for by the controller without a disturbance model. This approach has been demonstrated in many exosuits (Georgarakis et al., 2022; Wu et al., 2018; Xiloyannis et al., 2019). Georgarakis and colleagues showed that the tension tracking root mean square error (RMSE) can be brought as low as 3.4 N (16%, this percentage value has been computed based on the original data available to the authors) during trajectories that represent activities of daily living (ADLs) patterns (Georgarakis et al., 2020).

However, force-sensing devices add cost and complexity to the system, require careful tuning, and add distal components. The overall system complexity makes the technology transfer from academia to industry challenging (Tong, 2018). Furthermore, the presence of distal components may make the device more cumbersome to wear, lowering its acceptability (Ang et al., 2023).

## **1.2. Friction modeling and compensation**

Frictional losses in Bowden-sheath transmission are non-negligible, particularly when the sheath undergoes bending. Additionally, the material properties of the sheath and cable can significantly impact the efficiency of the transmission (Chen et al., 2014). Several models have been proposed to characterize the disturbances inside Bowden transmissions and compensate for them. Many of these are dynamic models based on Coulomb friction and the Capstan formula, often including the elastic behavior of the system (Agrawal et al., 2010; Buchanan and Sergi, 2021; Wu et al., 2019).

Since this friction is highly dependent on the cable-sheath bending angle, Jeong et al. explored loop routing as a method to make the frictional disturbance more constant with positional changes of the end effector relative to the actuator of a two-dimensional manipulator robot (Jeong and Cho, 2015). Although perhaps counterintuitive, increasing the magnitude of the disturbance in order to reduce its variability made a feed-forward compensation strategy effective. Nevertheless, loop-routing may not be the best strategy for wearable robots, as extra loops in the transmission might introduce snag points resulting in a less discrete suit design. Moreover, a decrease in the efficiency of the transmission would require a higher magnitude of motor torque negatively impacting motor dimensions and weight as well as energy consumption and battery life.

Removing the load cell from cable-driven upper limb rigid exoskeletons has been recently attempted by some research groups (Dežman et al., 2022; Orekhov et al., 2020; Zhang et al., 2020). For example, Zhang et al. designed an actuation unit used within a 4 degree of freedom (4-DOF) arm exoskeleton, which includes a compact rotary series elastic actuator and Bowden cable with a simplified Bowden-sheath friction model in order to estimate the frictional losses in the transmission (Zhang et al., 2020). To the best of our knowledge, no upper limb cable-driven exosuits implement load-cell-free tension control.

### 1.3. Objective

The objectives of this work are twofold:

1. to remove the load cell from the control architecture of a cable-driven upper limb exosuit and to prove the feasibility of the approach and
2. to assess the efficacy of the novel exosuit and control approach in supporting humeral elevation movements in healthy participants.

This paper presents a design and model-based control approach to remove the load cell from a cable-driven exosuit. A straightforward and reproducible friction model identification procedure was conducted. This was integrated in a model-based tension controller to regulate the cable tension of the exosuit. The feasibility of the approach was proven on healthy participants by assessing the ability of the controller to track the desired tension at different movement speeds and levels of support. The efficacy of the exosuit was also investigated by evaluating muscular activation via surface electromyography (sEMG) and movement kinematics with and without the suit. Additionally, the comfort and perceived physical exertion were assessed through questionnaires.

## 2. Materials and methods

### 2.1. Exosuit design

The exosuit designed for this study was composed of:

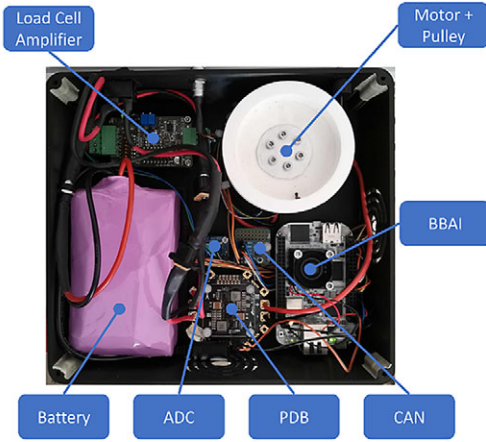
1. a TDU (Figure 1a),
2. a cable and Bowden sheath used to transmit forces from the TDU into supportive torques on the arm (Figure 1b), and
3. textile components to secure the TDU and cable to the body of the user.

The TDU actuator was a brushless DC motor (AK60–6 V1.1, T-motor, China) with a three-dimensional (3D)-printed polylactic acid (PLA) spool with a diameter of 70 mm. This quasi-direct drive (QDD) motor has a reduction of 6:1 and offers a wider control bandwidth and improved torque control with respect to high-gear-ratio brushless DC motors (Yu et al., 2020).

The microcontroller was a BeagleBone AI (BeagleBoard.org, Oakland Twp, MI) using a controller area network bus (SN65HVD230 3.3 V breakout module, Arduino) for motor communications. A 24-V, 7-Ah lithium-ion battery (Seilylanka) provided power which was distributed with a power distribution board (PDB500, Advanced Power Drives, PL, Australia). The humeral angle of elevation was measured with an inertial measurement unit (IMU) strapped to the upper arm (NGIMU, x-io Technologies, UK). A load cell (LSB201, Futek, CA, USA), signal amplifier (IAA100, Futek, CA, USA), and analog-to-digital converter (16-bit ADS1115, Adafruit Industries, NY, USA) were used to measure cable tension. The load cell was not used in the controller but to identify the model parameters and for evaluation purposes.

A backpack frame (B and W International BPS/5000) and an arm cuff designed by Georarakis et al. (2022) were used as textile components. The TDU was attached at the lumbar level to keep the system weight closer to the center of mass of the user.

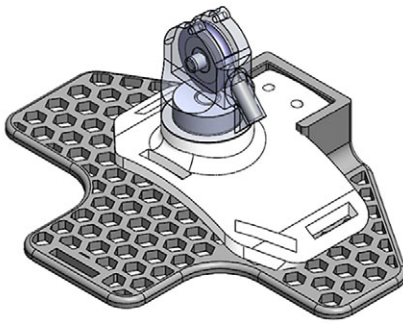
The cable (1.5 mm Dyneema cable, ExtremTextil) was guided through a Bowden sheath (Slickwire, SRAM), selected for its high stiffness based on the recommendations from Chen et al. (2014). The cable exit was secured above the shoulder with a PLA 3D-printed shoulder cuff (Figure 1c) designed to minimize frictional losses. The cuff has a bearing to adapt to the humeral plane-of-elevation (defined according to the International Society of Biomechanics (Wu et al., 2005) and a pulley at the end of the Bowden sheath to redirect the cable to minimize the bending angle of the sheath.



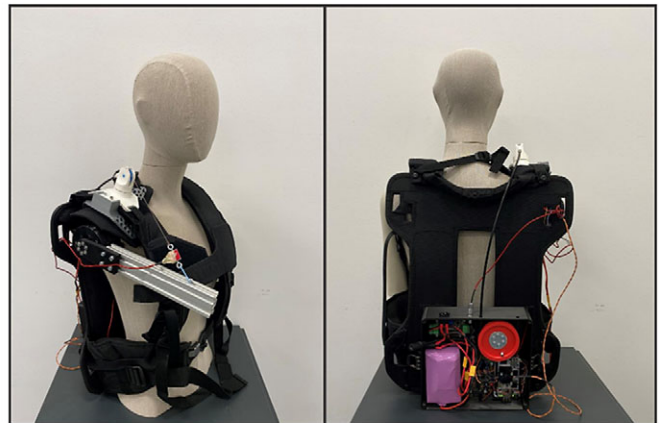
(a)



(b)



(c)



(d)

**Figure 1.** (a) Picture of the TDU in the final assembled configuration with major electromechanical components labeled. (b) Functioning principle of the exosuit. Cable tension, generated in the TDU by the motor, is transmitted along the body through the Bowden-sheath system. This results in an assistive torque about the glenohumeral joint of the wearer, supporting the arm against gravity. (c) Rendering of the swivelling shoulder cuff in Solidworks 2021. (d) Setup for the model identification experiments. The mannequin, modified with a motorized arm, wears the exosuit.

## 2.2. Modeling and identification

### 2.2.1. Transmission model

The transmission model maps the desired motor torque ( $\tau_{des}$ ) to the cable tension acting on the arm ( $T_{out}$ ). Inertial effects were assumed negligible since a QDD motor was used. The input tension ( $T_{in}$ ) is related to the desired motor torque and spool radius ( $R_p$ ):

$$T_{in} = \frac{\tau_{des}}{R_p} \tag{1}$$

The output tension ( $T_{out}$ ) of a Bowden-sheath system is:

$$T_{out} = T_{in} \left( 1 - \operatorname{sgn}(V_{cable}) \frac{2\mu \sin(\frac{\phi}{2})}{1 + \operatorname{sgn}(V_{cable})\mu \sin(\frac{\phi}{2})} \right) \quad (2)$$

where  $V_{cable}$  is the relative velocity between the cable and sheath,  $\mu$  is the Coulomb friction coefficient, and  $\phi$  is the sheath total wrapping angle. The full derivation of Equation (2) is reported in Section 1 of Supplementary Materials. From this equation, it may be seen that in a friction-free scenario, the output tension would equal the input tension. With friction, the output tension changes according to the sign of the cable velocity. With a positive cable velocity (raising the arm), the magnitude of the output tension will be less than the magnitude of the input tension, as the term in brackets in Equation (2) will be less than 1. This results in less support being delivered to the arm. With a negative cable velocity (lowering the arm), the magnitude of the output tension will be greater than the magnitude of the input tension, as the term in brackets in Equation (2) will be greater than 1. This results in a perceived resistance when lowering the arm. In both cases (raising and lowering the arm), the output tension is linearly proportional to the input tension, assuming that  $\mu$  and  $\phi$  are constant with time, but with a constant of proportionality that depends on the direction of cable travel.

### 2.2.2. Proposed inverse transmission model

To compute the motor torque ( $\tau_{des}$ ) necessary to achieve a desired output cable tension ( $T_{out,des}$ ), the following inverse transmission model is proposed:

$$\begin{cases} \tau_{des,lowering} = b_{lowering} + m_{lowering} \cdot T_{out,des}, & \text{if } V_{cable} < 0 \\ \tau_{des,raising} = b_{raising} + m_{raising} \cdot T_{out,des}, & \text{if } V_{cable} > 0 \end{cases} \quad (3)$$

These linear models are characterized by a slope ( $m$ ) and intercept ( $b$ ). The subscripts *raising* and *lowering* are used to differentiate the two lines. The model is based on the insights presented in Section 2.2.1. For the user to feel the same output tension (for a fixed input tension) when raising or lowering the arm, the motor must deliver more or less torque, respectively.

### 2.2.3. Data acquisition

A motorized human-like mannequin test bench was developed for the identification procedure (Figure 1d). The TDU motor was controlled in trajectory to achieve a set of quasi-constant spool velocities ( $\pm 0.5, 1, 2, 3, 4, 5,$  and  $6$  rad/s) across the range of motion (from  $20$  to  $110^\circ$ ) of the driven arm. Each velocity condition was repeated five times. The mannequin motor was controlled in torque to apply a set of constant loads ( $0.5, 1, 2, 3,$  and  $4$  Nm) for each velocity condition.

### 2.2.4. Model identification

The output tension measured by the load cell ( $T_{out}$ ), the estimated torque applied by the TDU motor ( $\tau_m$ ), and the velocity estimated from the motor encoder were filtered with a zero-phase third-order low-pass Butterworth filter with a cutoff frequency of  $5$  Hz. To take into account only data acquired in steady-state conditions, a set of conditions was applied to select relevant data points:

- $TDU_{speed} > 15^\circ/s,$
- $TDU_{acc} < 15^\circ/s,$
- $20^\circ < \theta_{AOE} < 90^\circ,$
- $TDU_{torque} > 0\text{Nm},$

where  $TDU_{speed}$  is the TDU motor speed,  $TDU_{acc}$  is the TDU motor acceleration,  $\theta_{AOE}$  is the mannequin humeral angle of elevation estimated by the IMU, and  $TDU_{torque}$  is the TDU motor torque.

The data was split into the raising and lowering phases based on the velocity of the TDU motor. The parameters of the inverse transmission model defined in Section 2.2.1 ( $b_{lowering}$ ,  $m_{lowering}$ ,  $b_{raising}$ , and  $m_{raising}$ ) were computed from two linear fittings between the output cable tension and the motor torque. This was carried out in MATLAB R2023a (Mathworks Inc.) using the *robustfit* function.

### 2.3. Control architecture

The TDU controller represented in Figure 2 works in the following fashion:

1. A gravity assistance block computes the desired cable tension ( $T_{out,des}$ ) from the humeral angle of elevation ( $\theta_{AOE}$ ). The gravity assistance model is detailed in Supplementary Material – Section 2.
2. The transmission inverse model and friction compensation block, identified in Section 2.2.4, compute the desired motor torque ( $\tau_{des}$ ) from both the desired cable tension ( $T_{out,des}$ ) and the elevation velocity of the arm ( $\dot{\theta}_{AOE}$ ). The sign of the arm elevation velocity is used as a proxy for the sign of the cable velocity to anticipate changes in direction.
3. An open-loop torque controller embedded in the motor takes the desired torque ( $\tau_{des}$ ) as input and controls the motor phase currents to achieve a motor output torque ( $\tau_m$ ).
4. The motor output torque acts on the cable through the spool and is transmitted to the arm through the Bowden-sheath mechanism. The position of the arm is sensed by the IMU and used as input for the gravity assistance model. The arm elevation velocity is computed in real time on the TDU, first using a second-order 10 Hz, cutoff low-pass Butterworth filter, and then a four-point backwards finite differences filter.

To ensure a smooth transition of the commanded torque depending on the arm velocity, a sigmoid was applied to link the two regression lines:

$$\tau_{des} = \tau_{des,lowering} + \frac{\tau_{des,raising} - \tau_{des,lowering}}{1 + e^{-B \cdot (\dot{\theta}_{AOE} - M)}} \tag{4}$$

The shape parameters of the sigmoid coupling function ( $M$  and  $B$ ) can be set by fixing the humeral elevation velocities at which 1 and 99% of the sigmoid extremal values should be achieved ( $\dot{\theta}_{AOE,001}$  and  $\dot{\theta}_{AOE,099}$ , respectively):

$$M = \frac{\dot{\theta}_{AOE,001} + \dot{\theta}_{AOE,099}}{2} \tag{5}$$

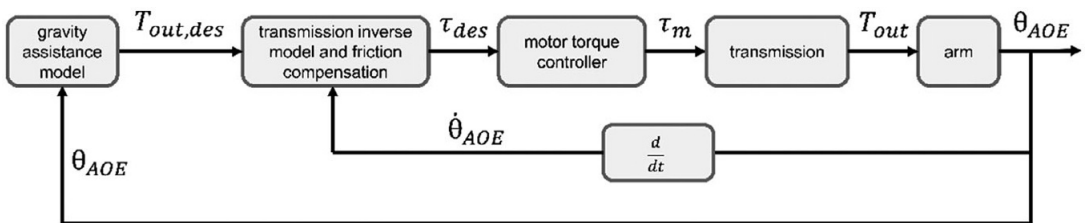


**Figure 2.** Control block diagram developed for this study.  $T_{out,des}$  is the desired output tension of the tendon acting on the arm cuff.  $\tau_{des}$  is the desired motor torque.  $\tau_m$  is the actual motor torque delivered to the spool.  $T_{out}$  is the actual tendon tension delivered to the cuff.  $\theta_{AOE}$  is the humeral angle of elevation as measured by the IMU.  $\dot{\theta}_{AOE}$  is the first time derivative of the humeral angle of elevation (elevation velocity).

$$B = \frac{\ln(99)}{\dot{\theta}_{AOE,001} - M} \quad (6)$$

For this study,  $\dot{\theta}_{AOE,001}$  and  $\dot{\theta}_{AOE,099}$  were set to  $-1$  and  $1$  rad/s, respectively. Altering the width of the sigmoid affects how quickly the compensation switches between raising and lowering movements, and shifting the sigmoid affects the amount of compensation while raising, lowering, and in static positions.

## 2.4. System evaluation tests on healthy participants

### 2.4.1. Protocol

To evaluate the feasibility of such a controller, experiments were conducted on healthy volunteers. The protocol (Figure 3) was approved by the ethical committee of Politecnico di Milano (opinion n. 46/2022, 16/11/2022). Each participant read and signed a written informed consent.

The task consisted of standing upright and tracking a forward humeral elevation reference trajectory shown on a screen while holding a 0.5-kg weight (Figure 4a). The actual humeral angle of elevation estimated by the IMU sensor was provided as feedback on the same screen. The minimum-jerk trajectory transitioned between  $20^\circ$  and  $100^\circ$  arm elevation and was repeated 10 times for each peak speed and support level. The participants were verbally instructed to keep the elbow fully extended, but relaxed.

The EMG electrodes were applied to the muscles involved in humeral elevation (Figure 4b): agonist muscles (anterior deltoid, medial deltoid, trapezius, and pectoralis major), antagonist muscles (posterior deltoid and latissimus dorsi), and elbow stabilizers (biceps and triceps), following the international SENIAM recommendations (Hermens et al., 1999). The reference and ground electrodes were placed on the lateral epicondyle of the humerus and the ulnar styloid process, respectively. The EMG acquisition system was a SAGA 32+/64+ (TMS International, The Netherlands) sampling the signal at a frequency of 2,000 Hz and synchronized with the TDU.

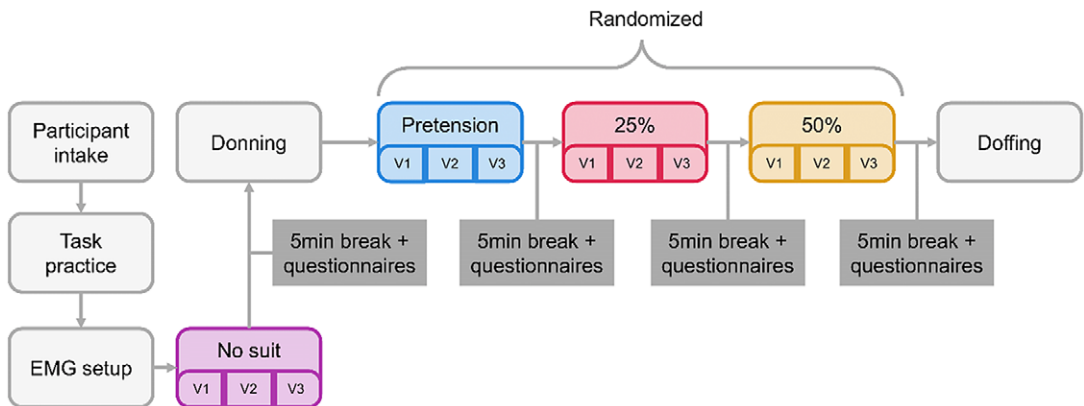


**Figure 3.** Study protocol. Participants were first explained the full protocol and had the opportunity to perform a training task without the suit for familiarization. The task was repeated for four conditions: no-suit (no), pretension of 10 N (pre), 25% gravity support (25%), and 50% gravity support (50%). The no-suit condition was always performed as the first to measure the baseline EMG values of each participant. The other three conditions were randomized in order to exclude effects from habituation to the device. A 5-min break was given to each participant between conditions while a set of questionnaires were administered. For each support condition, three movement speed conditions were tested. The slow condition had a peak speed of  $60^\circ/s$  (V1), the medium condition  $120^\circ/s$  (V2), and the fast condition  $180^\circ/s$  (V3). At the end of the study, the exosuit and EMG system was removed, and the participant thanked with a cookie.

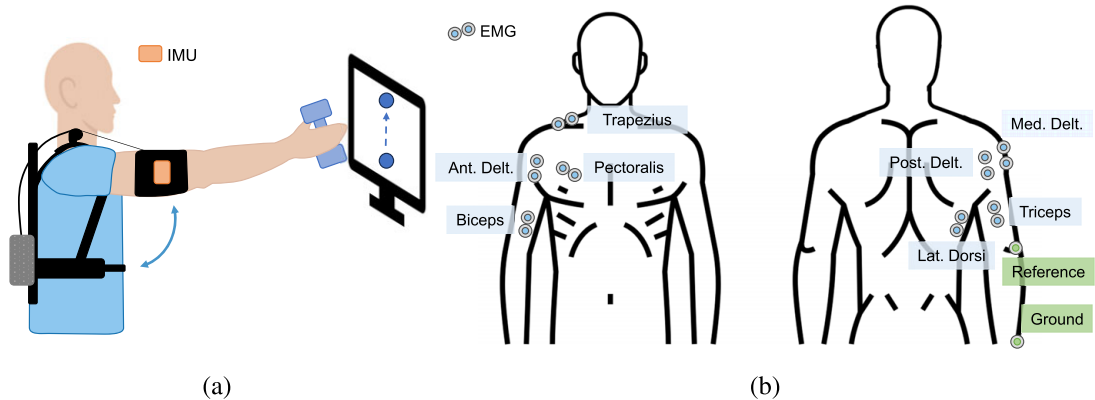


**Figure 4.** (a) Experimental setup and (b) EMG electrodes placement. This image has been designed using resources from *Flaticon.com*.

#### 2.4.2. Data processing

EMG data were pre-processed in MATLAB R2023a (Mathworks inc.) to extract the EMG envelopes of the selected muscles. A third-order zero-phase Butterworth bandpass filter (20–400 Hz) was applied to the raw data which was then rectified and smoothed with a sliding 100 ms-wide RMS window (Burden, 2017). Additionally, for the pectoralis major and the latissimus dorsi, the ECG artifact was removed by means of adaptive template subtraction with the Cardiac artifact removal toolbox (Petersen, 2023; Petersen et al., 2020). The first of 10 repetitions for each condition–velocity set was removed from the analysis because of adaptation effects happening at the beginning of the exercise when condition and/or speed were changed (Emken et al., 2007).

The EMG envelope amplitude was normalized to the average maximum peak of the no-suit condition, separately for each participant and velocity.

#### 2.4.3. Outcome measures

The following outcome measures were computed for each repetition:

- RMSE between the desired and the measured tension and torque to evaluate the controller tracking performance split in the raising and lowering phases;
- RMSE between the desired and the measured humeral angle of elevation and SPARC index (Balasubramanian et al., 2015) computed from the speed of humeral elevation estimated from the IMU ( $\dot{\theta}_{AOE}$ ) to evaluate the effect of the suit on the kinematics of the arm;
- average integral of the sEMG (iEMG) on a normalized time vector to evaluate the effect of the suit on the activation of the selected muscles split in the raising and lowering phases; and
- perceived discomfort (modified Nordic questionnaire from (Kuorinka et al., 1987)), perceived physical exertion (Borg Rate of Perceived Exertion, or RPE from (Borg, 1982)), and perceived muscular fatigue to evaluate the perception of the user. Details on the questionnaires can be found in Section 3 of Supplementary Materials.

#### 2.4.4. Statistical analysis

Generalized linear mixed models were defined in SPSS Statistics 28 (IBM) to evaluate whether the iEMG (split into raising, lowering, and entire movement cycle) of each muscle, the humeral elevation angle RMSE, and the SPARC-index were significantly different across conditions and speeds without the assumption of normality, taking into account repeated measures and multiple effects. In the analysis, the iEMG, the RMSE, and the SPARC index were considered as the target for each model following a gamma regression distribution with a log link to the linear model. Condition, speed, and the interaction of the two were considered fixed



effects while the participants were considered as random effects by associating their ID to the intercept with a variance component covariance type. A pairwise comparison with the sequential Bonferroni correction for multiple comparisons was conducted on the effects that showed a p-value lower than .05.

The questionnaire results were compared across conditions by means of a Friedman test in MATLAB R2023a (Mathworks Inc.). If the p-value was lower than 0.05, a pairwise comparison was conducted by means of the *multcompare* function applying the Bonferroni correction for multiple comparisons.

### 3. Results

#### 3.1. Model identification on mannequin

The identified regression lines for raising and lowering had a goodness of fit of .9940 and .9906, respectively (Figure 5). The slopes and the intercepts of the two regression lines were used in the control strategy described in Section 2.3.

#### 3.2. System evaluation experiments on healthy participants

Eighteen healthy volunteers (12 F/6 M) were recruited for the study. The experiment was interrupted for one participant due to electrode detachment and discontinued. The participants' mean age was 29.33 years (SD = 7.04), the mean height was 1.70 m (SD = 0.11), and the mean weight was 63.23 kg (SD = 11.51).

For each participant, the humeral angle of elevation, the supportive torque, the cable tension, and the muscle sEMG were measured. The data was averaged over the nine repetitions and resampled onto a normalized time vector for each participant, condition, and speed (Figure 6).

##### 3.2.1. Assistive tension and torque tracking

The shoulder torque RMSE and cable tension RMSE increased with support and velocity for the entire movement cycle. The overall torque RMSE ranged from a minimum of 0.29 to 0.90 Nm, while the cable tension RMSE ranged from a minimum of 2.75 to 9.07 N (Table 1). If considered as percentage errors

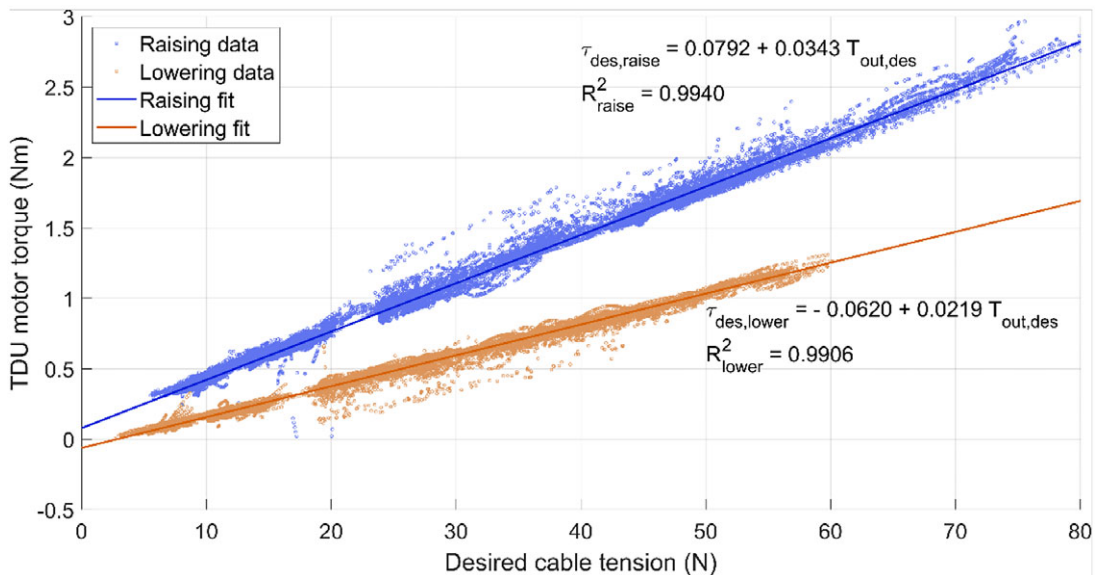


**Figure 5.** Linear regressions of the desired cable tension ( $T_{out,des}$ ) and the TDU motor torque ( $\tau_{des}$ ) required. The graph axes are presented this way to reflect the controller architecture (Figure 2). The data and regression line for the raising phase is shown in blue, while the lowering phase is shown in orange. Slope and intercept are displayed along with goodness of fit ( $R^2$ ).

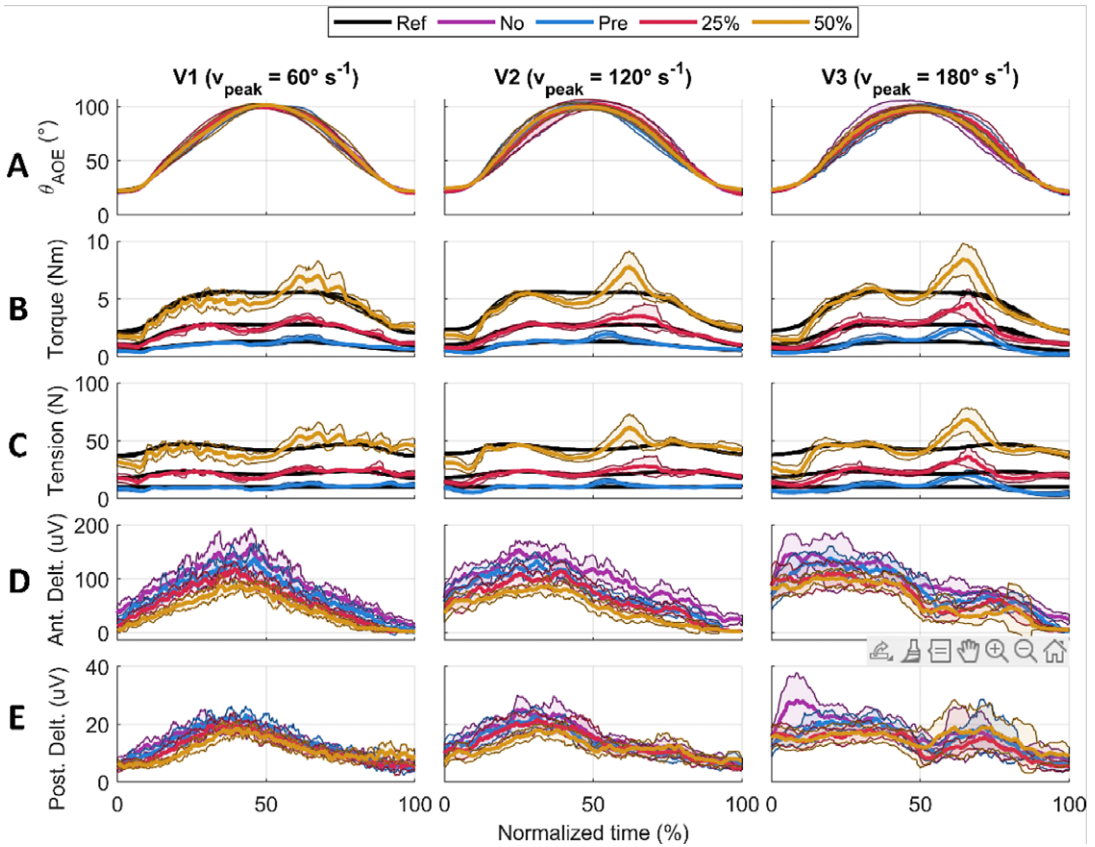


**Figure 6.** Results for one participant averaged over the nine repetitions. The solid lines represent the average value, the shaded area is the standard deviation. Each column shows a velocity condition (V1, V2, and V3). The rows show humeral angle of elevation (a), shoulder supportive torque (b), output cable tension (c), anterior deltoid EMG (d), and posterior deltoid EMG (e).

**Table 1.** Torque and tension tracking RMSE presented for all combinations of velocities and support conditions, averaged across all participants

	V1 ( $v_{peak} = 60^\circ/s$ )			V2 ( $v_{peak} = 120^\circ/s$ )			V3 ( $v_{peak} = 180^\circ/s$ )		
	Entire	Raise	Lower	Entire	Raise	Lower	Entire	Raise	Lower
Torque RMSE (Nm)									
Pre	0.29	0.23	0.32	0.40	0.25	0.47	0.69	0.43	0.84
25%	0.42	0.38	0.44	0.58	0.41	0.68	0.74	0.50	0.91
50%	0.66	0.64	0.66	0.71	0.54	0.82	0.90	0.57	1.11
Tension RMSE (N)									
Pre	2.75	2.37	2.98	3.58	2.90	3.92	6.15	4.51	7.20
25%	4.09	3.83	4.14	5.31	4.70	5.61	6.74	5.70	7.47
50%	6.14	6.03	6.10	6.46	5.94	6.72	8.17	6.80	9.07

Note. The results are further split showing the average RMSE of the entire arm cycle, the raising portion, and the lowering portion.

compared to the reference signal, these errors were 27.5 and 23.4%, respectively (see Supplementary Material Table S1).

When considering the movement split into the raising and lowering phases, the torque and tension RMSE values were always higher when lowering. Peaks in the applied torque and tension exceeding the

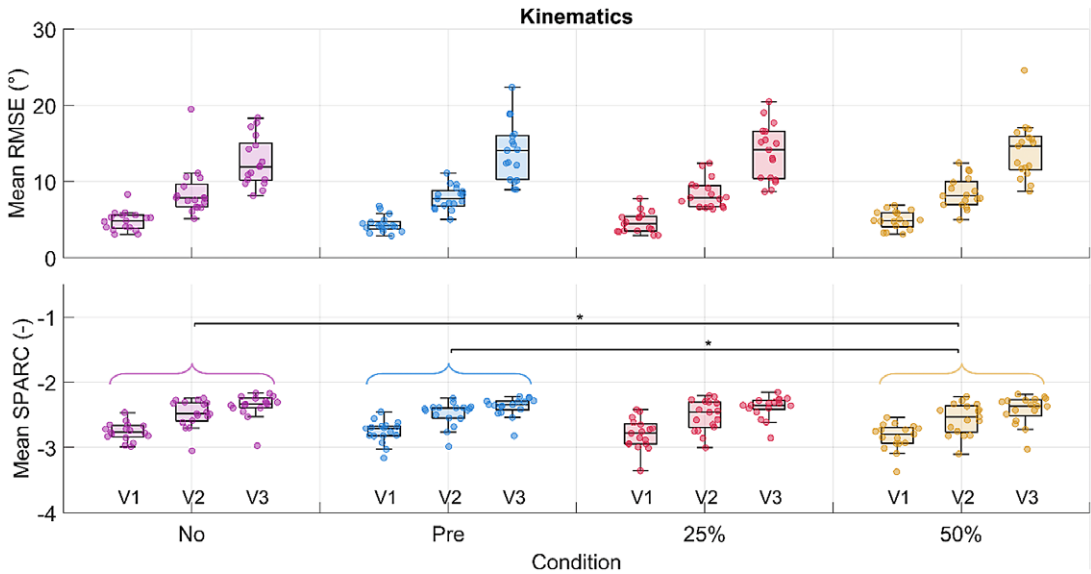


**Figure 7.** RMSE and SPARC for the humeral angle of elevation are shown in the first and second rows, respectively. Each dot in each boxplot represents one participant. The results are shown subdivided by velocity but the statistical significance level for the pairwise comparison among conditions is shown for the velocities grouped. The following significance codes are used to represent the according ranges of  $p$  values for the post hoc tests:  $**[0, .001)$ ,  $*[.001, .05)$ .

reference were observed around the onset of lowering at approximately 60% of the normalized time of the entire movement (Figure 6b and c, see Supplementary Material Tables S2 and S3 for computed average values).

### 3.2.2. Trajectory tracking and smoothness

A significant difference in the condition effect was found for the SPARC index between the no-suit and the 50% gravity support conditions, and the pretension and the 50% gravity support conditions (Figure 7). SPARC decreased significantly by 3% between the no-suit and the 50% gravity support conditions. As for the velocity effect, a significant difference was found both for the RMSE and the SPARC index. No difference was found in the interaction of condition and velocity for both outcomes (detailed results are reported in Supplementary Material Tables S4, S5, and S6).

### 3.2.3. EMG

Significant differences in the condition and velocity effects were found across the muscles both in the raising and lowering phases. No differences were found for the interaction effect of condition and velocity (see Supplementary Material Tables S7, S8, and S9).

Significant decreases in the iEMG from the no-suit condition to the various support conditions were detected for the anterior deltoid (Figure 8), trapezius, and pectoralis major during the raising and lowering phases along with the entire movement cycle. The greatest changes happened between the no-suit and 50% support conditions. The anterior deltoid, trapezius, and pectoralis major activities decreased by 30, 38, and 38% during raising and 39, 42, and 35% during lowering, respectively.

The posterior deltoid activity increased significantly by 32% during lowering (Figure 9). Other muscles, such as the medial deltoid and latissimus dorsi, showed some significant differences, though the trends across all post hoc tests were less clear (changes visualized for all muscles in Tables 2 and 3, see Supplementary Material Tables S10, S11, and S12 for numerical values).

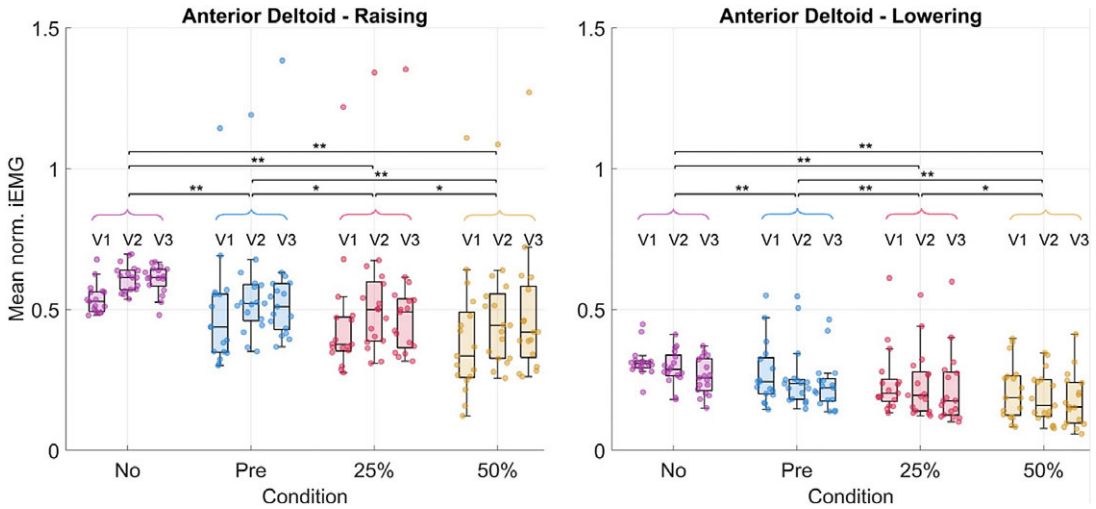


**Figure 8.** Results in terms of mean normalized iEMG for the anterior deltoid. Each dot in each boxplot represents one participant. The results are shown subdivided by velocity but the statistical significance level for the pairwise comparisons between conditions is shown for the velocities grouped. The following significance codes are used to represent the according ranges of p values for the post hoc tests: \*\*[0, .001), \*[.001, .05).

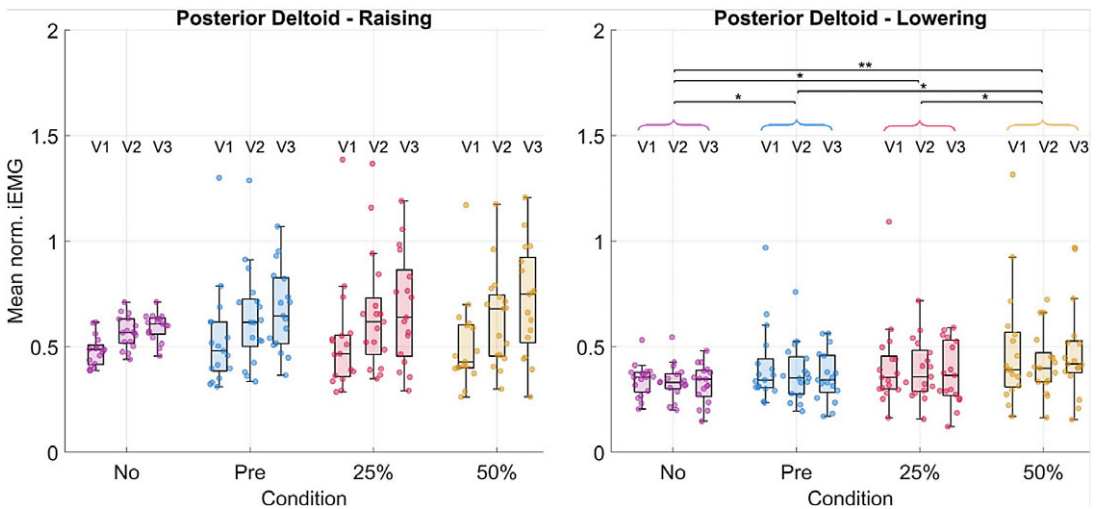


**Figure 9.** Results in terms of mean normalized iEMG for the posterior deltoid. Each dot in each boxplot represents one participant. The results are shown subdivided by velocity but the statistical significance levels for the pairwise comparisons between conditions are shown for the velocities grouped. The following significance codes are used to represent the according ranges of p-values for the post hoc tests: \*\*[0, .001), \*[.001, .05).

**3.2.4. Questionnaires**

Significant changes in discomfort in the lower neck (p = .001) and right shoulder (p = .001) were highlighted by the statistical analysis of the Nordic questionnaire outcomes (Figure 10). In particular, the discomfort in the lower neck area significantly increased from the no-suit condition to the pretension (p = .027), 25% (p = .002), and 50% (p = .006) support conditions. The discomfort in the shoulder area

**Table 2.** EMG statistical results for the pairwise post hoc tests comparing changes in muscular activity across all muscle groups for the raising portion of the arm cycle

Muscle group	Raising phase					
	Pre-no	25%-no	50%-no	25%-pre	50%-pre	50–25%
Anterior deltoid	**	**	**	*	**	*
Medial deltoid					**	*
Posterior deltoid						
Biceps	*	*				
Triceps					*	
Trapezius	**	**	**	*	**	**
Latissimus dorsi			*		*	*
Pectoralis major	**	**	**		**	**

Note. The following significance codes are used for the p values: \*\*[0, .001), \*[.001, .05), and a blank space represents [.05, 1]. The percentage changes in normalized iEMG, relative to the second condition being compared, is coded in color, with green representing a decrease in iEMG from the second to the first condition, and red representing an increase.

**Table 3.** EMG statistical results for the pairwise post-hoc tests comparing changes in muscular activity across all muscle groups for the lowering portion of the arm cycle

Muscle group	Lowering phase					
	Pre-no	25%-no	50%-no	25%-pre	50%-pre	50–25%
Anterior deltoid	**	**	**	**	**	**
Medial deltoid					**	*
Posterior deltoid	*	*	**		*	*
Biceps	*	*			*	
Triceps						
Trapezius	**	**	**		*	
Latissimus dorsi						
Pectoralis major	*	*	**		*	

Note. The following significance codes are used for the p values: \*\*[0, .001), \*[.001, .05), and a blank space represents [.05, 1]. The percentage changes in normalized iEMG, relative to the second condition being compared, is coded in color, with green representing a decrease in iEMG from the second to the first condition, and red representing an increase.

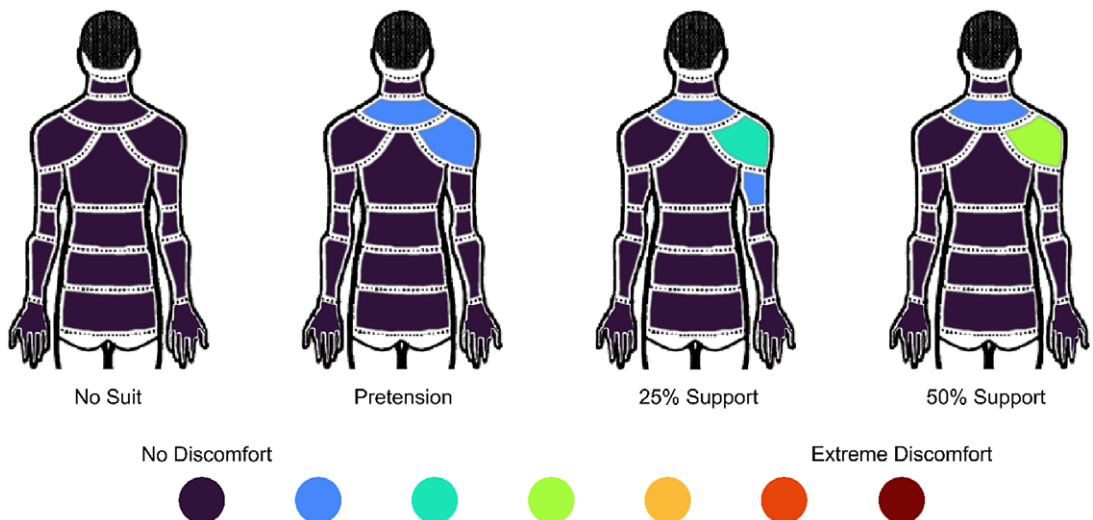


**Figure 10.** Modified Nordic questionnaire results reporting median score across all participants. The figure is viewed from behind, and the right arm was supported by the exosuit.

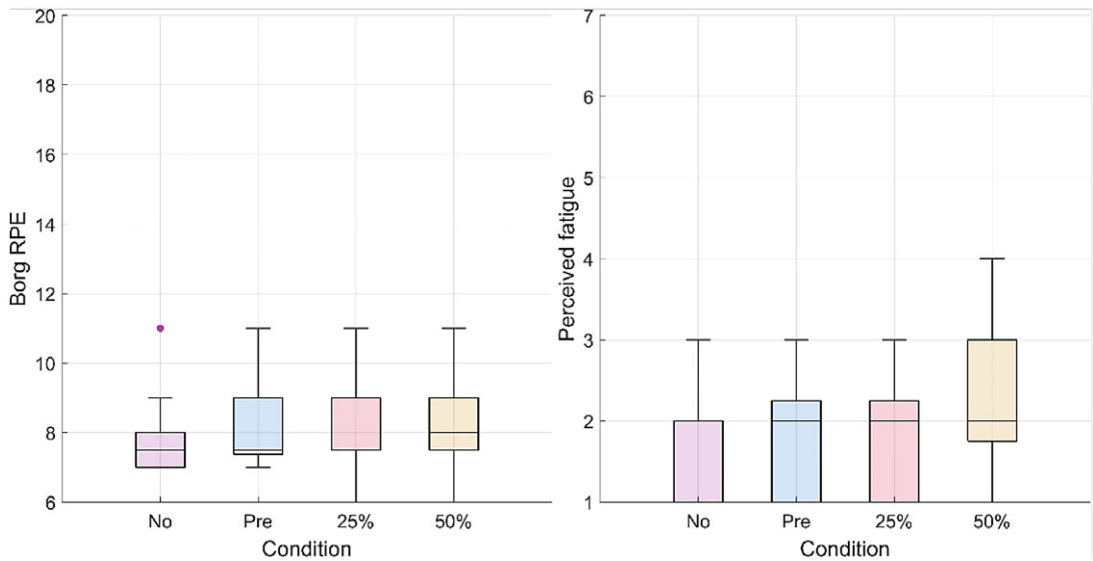


**Figure 11.** Box plots representing the questionnaire results for the RPE (on the left) and perceived muscular fatigue for the deltoid group (on the right). For the RPE, 6 corresponds to the lowest score on the scale (“No exertion at all”) and 11 corresponds to an RPE of “Light.” The scale goes up to 20 (“Maximal exertion”). For perceived muscular fatigue, 1 corresponds to the lowest score on the Likert-type scale (“No Fatigue”) and 7 corresponds to the highest score (“Extreme Fatigue”).

significantly increased from the no-suit condition to the 25% ( $p = .002$ ), and 50% ( $p < .001$ ) support conditions and also from the pretension condition to the 50% support condition ( $p = .007$ ).

The RPE did not change significantly ( $p = .125$ ) as well as the muscular fatigue for all muscle groups (deltoids,  $p = .859$ ; pectoralis major,  $p = .801$ ; trapezius,  $p = .397$ ; biceps,  $p = .691$ ; latissimus dorsi,  $p = .488$ ; triceps,  $p = .475$ ) across conditions (Figure 11).

## 4. Discussion

### 4.1. Model identification

The developed model predicts a linear relationship between the desired output tension and the torque the TDU must apply to achieve that tension. During raising, the TDU motor must supply a higher torque to overcome the frictional losses in the transmission. On the contrary, when lowering, it is the arm of the user that must overcome the frictional losses in the transmission; hence, the TDU motor must provide less torque accordingly. The two regression lines identified and used in the control strategy had high goodness of fit, validating the proposed model.

### 4.2. System evaluation experiments on healthy participants

#### 4.2.1. Assistive tension and torque tracking

At the 50% support condition, the average RMSE was 6.14 N (17.4%), 6.46 N (18.2%), and 8.17 N (23.4%), for velocities V1, V2, and V3, respectively. Georgarakis et al. reported a mean RMSE for tension tracking of 3.4 N (16.1%) ( $n = 5$ ) when supporting 70% of the weight of the upper arm using a load cell to measure the cable tension and a tuned indirect force controller (Georgarakis et al., 2020). In terms of the RMSE errors, the controller developed by Georgarakis slightly outperforms the one developed in this paper. However, these results were achieved without a load cell to explicitly regulate the error in cable tension.

Moreover, further optimizations are proposed that could improve the controller performance. The spike in cable tension error around 60% of the movement cycle was a result of the transmission and motor stiction when the arm and cable changed direction. More complex modeling could capture the dynamics of stiction, or further mechanical optimizations could explore Bowden-sheath-free cable transmissions (such as redirect pulleys). A more thorough exploration of the sigmoid coupling parameters in [Section 2.3](#) may also reduce the effect of this disturbance. Finally, the perceptions of the users should be evaluated to better characterize the requirements in terms of tension tracking accuracy.

So far no works have reported the magnitudes of errors for the supportive torques at the shoulder joint for upper-limb exosuits. These values may be used by the community as a reference and additionally may be compared between devices regardless of actuation modality.

#### 4.2.2. Trajectory tracking and smoothness

The RMSE in the trajectory tracking was not significantly affected by the presence of the suit and the increasing support. On the contrary, movement smoothness decreased significantly with increasing exosuit support, indicating that the exosuit slightly interfered with the natural motion of the user. As all participants were healthy, and the task of lifting a 0.5-kg weight was relatively easy, it is possible that the higher supports disturbed movement smoothness, since the assistance was not necessary to perform the task.

#### 4.2.3. EMG

The anterior deltoid, trapezius, and pectoralis major demonstrated the strongest decreases ( $-30$ ,  $-38$ , and  $-38\%$ , respectively) in muscular activity with 50% gravity assistance of the exosuit. These results are comparable with those obtained by Georgarakis et al. (2022) in which the activity of the anterior deltoid and trapezius was reduced by  $-42$  and  $-49\%$ , respectively, when supporting the limb with 70% gravity assistance. Also Missiroli et al. (2022) achieved similar results with their hybrid occupational exoskeleton with a decrease of the activity of the anterior deltoid by  $-31\%$  when abducting the upper arm with passive support. As the exercise was a forward humeral elevation, one may expect to see decreased activity in these muscle groups as they are primarily responsible for supporting the arm against gravity. The activation of the posterior deltoid increased particularly ( $+32\%$ ) during the lowering phase of the movement. This indicates that the suit was impeding the lowering motion and that the posterior deltoid activity had to increase to compensate for this. It is likely that the spikes in supportive torque ([Figure 6](#)) observed at the onset of lowering could be the cause of this increase in muscular activity.

#### 4.2.4. Questionnaires

Mild discomfort was perceived in the upper neck for all exosuit support levels, and mild-to-moderate discomfort in the right shoulder was perceived as the support level was increased. This discomfort is likely a result of the pressure of the shoulder cuff on the upper neck and shoulder during support. These results might have been exacerbated by the presence of the EMG system, as electrodes were placed on the trapezius and on the deltoid groups underneath the exosuit cuff. Nevertheless, more efforts should be invested in designing a comfortable shoulder cuff and exploring if the pressure could be tolerated by stakeholders for long-term use.

No significant changes in RPE and perceived muscular fatigue were found with increasing support from the exosuit. The results from both questionnaires indicate a potential floor effect. A more physically demanding task might be necessary to elucidate differences in perceived exertion and muscular fatigue.

#### 4.2.5. Limitations and future improvements

One limitation of this study lies in the fact that some of the electrodes for recording sEMG needed to be placed underneath the exosuit meaning that different pressures could have been applied to the electrodes for each condition. However, a higher contact pressure generally does not influence wet electrode impedance (Taji et al., 2018). Increased discomfort may occur resulting from the higher pressures.

Regarding the movement task, since the focus of this paper was on control and sensing, only a single movement was explored (forward humeral elevation). Even if this movement is one of the most relevant for ADLs (Georgarakis et al., 2019), future studies should include movements performed in the context of specific activities. Moreover, humeral rotation and wrist flexion were not enforced strictly, so the participants could choose how to orient the weight during the motions.

Finally, the textile part of the exosuit was one-size-fits-all. Even though straps were adjustable, this led to fit issues, particularly for participants smaller in stature. Future iterations of the exosuit should include different textile and cuff sizes to adapt to each user.

## 5. Conclusion

Soft exosuits have the potential to mature into a technology that can support a broad range of users with muscular weakness, both during in-clinic rehabilitation and for daily assistance at home. The proposed design and control strategy entailed mechanical improvements to the TDU and cable transmission along with a model-based tension controller tuned through a simple data-driven friction identification procedure. The exosuit successfully reduced activation in the muscles responsible for arm elevation, without affecting the humeral elevation tracking error in healthy subjects. This established the feasibility of sensorless cable tension control. This work may be leveraged to further the development of simpler cable-driven exosuits, bringing them closer to people with muscular weakness and difficulties performing ADLs.

**Supplementary material.** The supplementary material for this article can be found at <http://doi.org/10.1017/wtc.2024.21>.

**Data availability statement.** All raw data and scripts for processing and analysis are available upon request. Please contact: [adrian.esser@hest.ethz.ch](mailto:adrian.esser@hest.ethz.ch)

**Acknowledgments.** The authors would like to thank Michi-Herold Nadig and Paul Schürmman for their support with integrating the electronics of the exosuit and Emanuele Bianchi for his support in developing the mannequin test bench. Additionally, the authors would like to express their thanks to the participants who volunteered their time and made this study possible.

**Author contribution.** E.B. and A.E. contributed equally to this work and share first authorship. Conceptualization, E.B. and A.E. Data curation, E.B. and A.E. Formal analysis, E.B. and A.E. Funding acquisition, P.W., M.G., E.A., A.P., and R.R. Investigation, E.B. and A.E. Methodology, E.B. and A.E.; Project administration, E.B. and A.E.; Resources, E.B. and A.E.; Software, E.B. and A.E.; Supervision, P.W., M.G., E.A., A.P., and R.R.; Validation, E.B. and A.E.; Visualization, E.B. and A.E.; Writing (Original Draft), E.B., A.E., P.W., M.G., E.A., A.P., and R.R. All authors approved the final submitted draft.

**Funding statement.** This work was supported as a part of NCCR Robotics, a National Centre of Competence in Research, funded by the Swiss National Science Foundation (grant number 51NF40\_185543). A travel grant was awarded to EB by IDEA League to support travel expenses.

**Competing interest.** M. Gandolla and A. Pedrocchi hold shares of AGADE srl and AllyArm srl.

**Ethical standard.** The protocol in this study was approved by the ethical committee of Politecnico di Milano (opinion n. 46/2022, November 16, 2022). Each participant read and signed a written informed consent prior to participation in the study.

## References

- Agrawal V, Peine WJ and Yao B (2010) Modeling of transmission characteristics across a cable-conduit system. *IEEE Transactions on Robotics* **26**(5), 914–924. <https://doi.org/10.1109/TRO.2010.2064014>
- Ang BW, Yeow Ch and Lim JH (2023) A critical review on factors affecting the user adoption of wearable and soft robotics. *Sensors (Basel)* **23**(3263), 1–22. <https://doi.org/10.3390/s23063263>
- Balasubramanian S, Melendez-Calderon A, Roby-Brami A and Burdet E (2015) On the analysis of movement smoothness. *Journal of NeuroEngineering and Rehabilitation* **12**. <https://doi.org/10.1186/s12984-015-0090-9>
- Bardi E, Gandolla M, Braghin F, Resta F, Pedrocchi AL and Ambrosini E (2022) Upper limb soft robotic wearable devices: a systematic review. *Journal of NeuroEngineering and Rehabilitation* **19**(1), 1–17.
- Bohannon RW (2007) Muscle strength and muscle training after stroke. *Journal of Rehabilitation Medicine* **39**(1), 14–20. <https://doi.org/10.2340/16501977-0018>
- Borg GA (1982) Psychophysical bases of perceived exertion. *Medicine and Science in Sports and Exercise* **14**(5), 377–381.



- Buchanan S and Sergi F** (2021) Dynamic modeling and state estimation of cable-conduit actuation during interaction with nonpassive environments. *IEEE/ASME Transactions on Mechatronics* **26**(5), 2462–2471. <https://doi.org/10.1109/TMECH.2020.3040159>
- Burden A** (2017) Surface electromyography. In Routledge, *Biomechanical Evaluation of Movement in Sport and Exercise*, chapter 5. Routledge London 116–139.
- Calanca A, Muradore R and Fiorini P** (2016) A review of algorithms for compliant control of stiff and fixed-compliance robots. *IEEE/ASME Transactions on Mechatronics* **21**(2), 613–624. <https://doi.org/10.1109/TMECH.2015.2465849>
- Chen D, Yun Y and Deshpande AD** (2014) Experimental characterization of Bowden cable friction. *Proceedings of IEEE International Conference on Robotics and Automation*, 5927–5933. <https://doi.org/10.1109/ICRA.2014.6907732>
- Choi H, Kang BB, Jung BK and Cho KJ** (2019) Exo-wrist: a soft tendon-driven wrist-wearable robot with active anchor for dart-throwing motion in hemiplegic patients. *IEEE Robotics and Automation Letters* **4**(4), 4499–4506. <https://doi.org/10.1109/LRA.2019.2931607>
- Das S and Kurita Y** (2020) ForceArm: a wearable pneumatic gel muscle (PGM)-based assistive suit for the upper limb. *IEEE Transactions on Medical Robotics and Bionics* **2**(2), 269–281. <https://doi.org/10.1109/tmrb.2020.2990436>
- Dežman M, Asfour T, Ude A and Gams A** (2022) Mechanical design and friction modelling of a cable-driven upper-limb exoskeleton. *Mechanism and Machine Theory* **171**, 104746. <https://doi.org/10.1016/j.mechmachtheory.2022.104746>
- Emken JL, Benitez R, Sideris A, Bobrow JE and Reinkensmeyer DJ** (2007) Motor adaptation as a greedy optimization of error and effort. *Journal of Neurophysiology* **97**(6), 3997–4006. <https://doi.org/10.1152/jn.01095.2006>
- Faria-Fortini I, Michaelsen SM, Cassiano JG and Teixeira-Salmela LF** (2011) Upper extremity function in stroke subjects: relationships between the international classification of functioning, disability, and health domains. *Journal of Hand Therapy* **24** (3), 257–265. <https://doi.org/10.1016/j.jht.2011.01.002>
- Georgarakis A-M, Song J, Wolf P, Riener R and Xiloyannis M** (2020) Control for gravity compensation in tendon-driven upper limb exosuits. *IEEE/RAS-EMBS International Conference on Biomedical Robotics and Biomechatronics*, 340–345. <https://doi.org/10.1109/BioRob49111.2020.9224460>
- Georgarakis AM, Xiloyannis M, Wolf P and Riener R** (2022) A textile exomuscle that assists the shoulder during functional movements for everyday life. *Nature Machine Intelligence* **4**(6), 574–582. <https://doi.org/10.1038/s42256-022-00495-3>
- Georgarakis AM, Wolf P and Riener R** (2019) Simplifying exosuits: kinematic couplings in the upper extremity during daily living tasks. *IEEE International Conference on Rehabilitation Robotics*, 423–428. <https://doi.org/10.1109/ICORR.2019.8779401>
- Hermens HJ, Freriks B, Merletti R, Stegeman D, Blok J, Rau G, Disselhorst-Klug C and Hägg G** (1999) *SENIAM 8: European recommendations for surface ElectroMyoGraphy*. *Roessingh Research Development* **24**, 13–55
- Hosseini M, Meattini R, San-Millan A, Palli G, Melchiorri C and Paik J** (2020) A sEMG-driven soft exosuit based on twisted string actuators for elbow assistive applications. *IEEE Robotics and Automation Letters* **5**(3), 4094–4101. <https://doi.org/10.1109/LRA.2020.2988152>
- Jeong U and Cho KJ** (2015) Feedforward friction compensation of Bowden-cable transmission via loop routing. *Proceedings of the IEEE/RSJ International Conference on Intelligent Robots and Systems*, 5948–5953. <https://doi.org/10.1109/IROS.2015.7354223>
- Kuorinka I, Jonsson B, Kilbom A, Vinterberg H, Biering-Sørensen F, Andersson G and Jørgensen K** (1987) Standardised nordic questionnaires for the analysis of musculoskeletal symptoms. *Applied Ergonomics* **18**(3), 233–237. [https://doi.org/10.1016/0003-6870\(87\)90010-X](https://doi.org/10.1016/0003-6870(87)90010-X)
- Longatelli V, Antonietti A, Biffi E, Diella E, D'Angelo MG, Rossini M, Molteni F, Boccione M, Pedrocchi A and Gandolla M** (2021) User-centred assistive SystEm for arm functions in neUromuscuLar subjects (USEFUL): a randomized controlled study. *Journal of NeuroEngineering and Rehabilitation* **18**(1), 1–17. <https://doi.org/10.1186/s12984-020-00794-z>
- Missiroli F, Lotti N, Tricomi E, Bokranz C, Alicea R, Xiloyannis M, Krzywinski J, Crea S, Vitiello N and Masia L** (2022) Rigid, soft, passive, and active: a hybrid occupational exoskeleton for bimanual multijoint assistance. *IEEE Robotics and Automation Letters* **7**(2), 2557–2564. <https://doi.org/10.1109/LRA.2022.3142447>
- Nätterlund B and Ahlström G** (2001) Activities of daily living and quality of life in persons with muscular dystrophy. *Journal of Rehabilitation Medicine* **33**(5), 206–211. <https://doi.org/10.1080/165019701750419590>
- Noronha B, Ng CY, Little K, Xiloyannis M, Kuah CWK, Wee SK, Kulkarni SR, Masia L, Chua KSG and Accoto D** (2022) Soft, lightweight wearable robots to support the upper limb in activities of daily living: a feasibility study on chronic stroke patients. *IEEE Transactions on Neural Systems and Rehabilitation Engineering* **30**, 1401–1411. <https://doi.org/10.1109/TNSRE.2022.3175224>
- Orehhov G, Luque J and Lerner ZF** (2020) Closing the loop on exoskeleton motor controllers: benefits of regression-based open-loop control. *IEEE Robotics and Automation Letters* **5**(4), 6025–6032. <https://doi.org/10.1109/LRA.2020.3011370>
- Petersen E** (2023) GitHub – ime-luebeck/ecg-removal: algorithms and evaluation toolkit for removing strong cardiac interference from surface EMG measurements – [github.com](https://github.com) (accessed 10 July 2023).
- Petersen E, Sauer J, Grabbhoff J and Rostalski P** (2020) Removing cardiac artifacts from single-channel respiratory electromyograms. *IEEE Access* **8**, 30905–30917. <https://doi.org/10.1109/ACCESS.2020.2972731>
- Proietti T., O'Neill C, Gerez L, Cole T, Mendelowitz S, Nuckols K, Hohimer C, Lin D, Paganoni S and Walsh C** (2023) Restoring arm function with a soft robotic wearable for individuals with amyotrophic lateral sclerosis. *Science Translational Medicine* **15**(681), eadd1504. <https://doi.org/10.1126/scitranslmed.add1504>

- Readioff R, Siddiqui ZK, Stewart C, Fulbrook L, O'Connor RJ and Chadwick EK** (2022) Use and evaluation of assistive technologies for upper limb function in tetraplegia. *Journal of Spinal Cord Medicine* **45**(6), 809–820. <https://doi.org/10.1080/10790268.2021.1878342>
- Taji B, Chan ADC and Shirmohammadi S** (2018) Effect of pressure on skin-electrode impedance in wearable biomedical measurement devices. *IEEE Transactions on Instrumentation and Measurement* **67**(8), 1900–1912. <https://doi.org/10.1109/TIM.2018.2806950>
- Tong R** (2018). *Wearable Technology in Medicine and Health Care*. Elsevier.
- Wang DX, Yao J, Zirek Y, Reijnierse EM and Maier AB** (2020) Muscle mass, strength, and physical performance predicting activities of daily living: a meta-analysis. *Journal of Cachexia, Sarcopenia and Muscle* **11**(1), 3–25. <https://doi.org/10.1002/jcsm.12502>
- Wu G, Van Der Helm FC, Veeger HE, Makhous M, Van Roy P, Anglin C, Nagels J, Karduna AR, McQuade K, Wang X, Werner FW and Buchholz B** (2005) ISB recommendation on definitions of joint coordinate systems of various joints for the reporting of human joint motion – part II: shoulder, elbow, wrist and hand. *Journal of Biomechanics* **38**(5), 981–992. <https://doi.org/10.1016/j.jbiomech.2004.05.042>
- Wu Q, Wang X, Chen B and Wu H** (2018) Design and fuzzy sliding mode admittance control of a soft wearable exoskeleton for elbow rehabilitation. *IEEE Access* **6**, 60249–60263. <https://doi.org/10.1109/ACCESS.2018.2875550>
- Wu Q, Wang X, Chen B and Wu H** (2019) Modeling, online identification, and compensation control of single tendon sheath system with time-varying configuration. *Mechanical Systems and Signal Processing* **130**, 56–73. <https://doi.org/10.1016/j.ymssp.2019.05.007>
- Xiloyannis M, Alicea R, Georgarakis AM, Haufe FL, Wolf P, Masia L and Riemer R** (2021) Soft robotic exosuits: state of the art, core technologies and open challenges. *IEEE Transactions on Robotics*, **38**, 1–20.
- Xiloyannis M, Chiaradia D, Frisoli A and Masia L** (2019) Physiological and kinematic effects of a soft exosuit on arm movements. *Journal of NeuroEngineering and Rehabilitation* **16**(1), 1–15. <https://doi.org/10.1186/s12984-019-0495-y>
- Yu S, Huang TH, Yang X, Jiao C, Yang J, Chen Y, Yi J and Su H** (2020) Quasi-direct drive actuation for a lightweight hip exoskeleton with high backdrivability and high bandwidth. *IEEE/ASME Transactions on Mechatronics* **25**(4), 1794–1802. <https://doi.org/10.1109/TMECH.2020.2995134>
- Zhang Q, Sun D, Qian W, Xiao X and Guo Z** (2020) Modeling and control of a cable-driven rotary series elastic actuator for an upper limb rehabilitation robot. *Frontiers in Neurorobotics* **14**, 13. <https://doi.org/10.3389/fnbot.2020.00013>